# Gravitational-wave Extraction using Independent Component Analysis

Rika Shimomura, Yuuichi Tabe, and Hisaaki Shinkai*
*Faculty of Information Science and Technology, Osaka Institute of Technology,*
*Kitayama 1-79-1, Hirakata City, Osaka 573-0196, Japan*
(Dated: March 18, 2025)

Independent component analysis (ICA) is a method to extract a set of time-series data using "statistical independency" of each component. We propose applying ICA for extracting gravitational wave (GW) signals. Our idea is to extract a signal that is commonly included in multiple detectors and to find it by shifting the data-set around its arrival time. In this article, we show several tests using injected signals, and show that this method can be applied to events for signal-to-noise over 15. We then demonstrate the method to actual O1-O3 events, and the identification of the arrival time can be estimated more precisely than that was previously reported. This approach does not require templates of waveform, therefore it can be applied for testing general relativity, and also for finding unknown GW.

## I. INTRODUCTION

Almost a decade has passed since the LIGO-Virgo collaboration directly detected the first gravitational wave (GW), GW150914 [1]. Up to this moment, the LIGO-Virgo-KAGRA (LVK) collaboration has reported 90 events as the GWTC-3 catalog, which is the result of the O3 observation period that was ended in March 2020[3]. The catalog consists of the 90 events from compact binary coalescences (CBCs), of which 85 events are from binary black-holes (BHs). LVK collaboration plans to announce the next catalog in coming months, in which we expect the number of detections double. In short, we are going to enter the era of GW astronomy.

As the number of events increases, we can discuss various aspects of astronomy and physics. For example, we are not sure how super-massive BHs in the center of galaxies were formed. This will require BH formation processes together with its formation rate and merging rate, which will be explained by GW statistics (see references in [4]). We are not sure how general relativity (GR) is unified with quantum theories. This viewpoint requires the validity of GR, of which best test can be performed in the strong gravity regimes, like the merger of BHs (see references in [5]).

GW signals are quite weak and often buried in the noisy outputs of detectors. The main method for detecting GWs from CBCs is the matched filtering analysis, which uses a template bank of waveforms and measures the correlation between a template and the observed signal. However, the method is only applicable for the prepared set of templates and is not effective for others. For example, GW searches of burst events from supernova explosions and/or stochastic events from phase transitions in the early Universe are not yet systematically performed due to the lack of templates. We are testing GR using templates based on GR, but are not possible to test other gravity theories. Therefore, it is desirable to develop a new method that can identify GW signals without using prepared templates.

Several new ideas have been proposed in this direction. One idea is to process time series data with mathematical and/or statistical techniques, or another is to use machine learning approaches (see a comparison of them for extracting ringdown mock data [6] and references therein). Such idea can be applied both for removing noises and for extracting GW signals, and is expected to be useful for supporting current standard data-analysis methods.

In this article, we propose one new idea for extracting GW signals, using independent component analysis (ICA) for extracting GW signals directly from the outputs of the detector data.

ICA is a method for separating a set of time series data into a new set, as its each component has "statistical independence" (see a review by Hyvärinen *et al.* [11, 12]). A well-known example is "blind signal separation", a method to identify the voices of $n$ persons in a cocktail party from their mixed sound files of $n$ microphones. See e.g. [13] for $n = 10$ case. ICA makes a linear representation of non-Gaussian data so as the components are statistically independent or as independent as possible. The fundamental measure is a separation how far from Gaussian. Thus, in the GW data analysis, we expect that GW extraction using ICA is effective, at least the background noise is Gaussian.

We note the differences between ICA and principal component analysis (PCA) of which applications to GW analysis have been reported recently in [7–10]. Both have a common goal to extract data as in the lower-dimensional space from original data, but their criteria are different. PCA is based on the principle of uncorrelation, by maximizing the variance of the data. On the other hand, ICA is based on statistical independency, in other words, no information can be obtained from other components, which is stronger requirement than uncorrelation. PCA is suitable for dimensional reduction to capture the main direction of large variance, data visualization, noise removal, etc, while ICA is effective for separating mixed signals and extracting hidden indepen-

* Contact author: hisaaki.shinkai@oit.ac.jp

dent components.

The usage of ICA to gravitational wave data analysis was first pointed out by De Rosa *et al.* [14]. The application to non-Gaussian noise subtraction was suggested by Morisaki *et al.* [16]. De Rosa *et al.* demonstrated ICA for injected signals mimicking two interferometer data, and reported that preprocessing ICA before matched filtering technique allows to lower the level of noise (increase the signal-to-noise ratio (SNR)). The KAGRA collaboration reported an application to their real data (iKAGRA data in 2016) for obtaining enhanced SNR using physical environmental channels (seismic channels) as known signals[15].

In this article, we report on our trials to extract GW signals directly using ICA. We demonstrate how injected data can be extracted from Gaussian noise, or from real detector output, and also show our trials of actual GW event data. GW events are fundamentally identified using data from multiple interferometers, taking into account the difference of the arrival time (up to 10 ms between Livingston and Hanford, 30 ms between Hanford and Virgo). We have developed a tool for extracting real GW signals which is available by shifting the data-set of multiple-detector data around its arrival time. In result, the arrival time differences between the detectors can be estimated more precisely than previously reported.

The structure of this article is as follows. In Section II, we explain the fundamental idea of ICA, and our basic procedures. In Section III, we demonstrate some tests using injected data for Gaussian noise and actual detector noise. In Section IV, we show the results of GW extractions of binary black-hole mergers in O1-O3. Our conclusions and outlook are given in Section V.

## II. INDEPENDENT COMPONENT ANALYSIS

### A. The fundamental procedures of ICA

Suppose we receive the time-series signal $\boldsymbol{x}(t) \equiv (x_1(t), \cdots, x_n(t))^T$ with $n$ detectors from $n$ source signals $\boldsymbol{s}(t) \equiv (s_1(t), \cdots, s_n(t))^T$, and they are mixed up linearly by

$$\boldsymbol{x}(t) = A\boldsymbol{s}(t), \tag{1}$$

where $A$ is the time-independent matrix which represents the superposition of the source signals. Our objective is to extract the source signal (candidate) $\tilde{\boldsymbol{s}}(t)$ from $\boldsymbol{x}(t)$. We write the problem as

$$\tilde{\boldsymbol{s}}(t) = W\boldsymbol{x}(t), \tag{2}$$

and set our goal to find out time-independent matrix $W$. We, heareafter, call $\boldsymbol{x}(t)$ and $\tilde{\boldsymbol{s}}(t)$ as input signals (to ICA) and output signals (from ICA), respectively.

ICA focuses on the idea of "statistical independence" of each source signal component $\tilde{\boldsymbol{s}}$. Roughly speaking, "statistical independence" can be evaluated as how far from Gaussianity. (Hence, ICA is not appropriate for extracting Gaussian signals since their superposition is Gaussian.)

Therefore, one strategy to search $W$ is

$$s_i(t) = \boldsymbol{w}_i^T V\boldsymbol{x}(t) \equiv \boldsymbol{w}_i^T\boldsymbol{z}(t) \tag{3}$$

has the most non-Gaussianity, where $\boldsymbol{w}_i^T = (w_{i1}, w_{i2}, \cdots)$ is a line of $W$, and $V$ expresses the whiten process of $\boldsymbol{x}(t)$ to $z(t)$ (which makes $\boldsymbol{x}(t)$ has no correlation and variance unity).

One possible measure of non-Gaussianity is the kurtosis of $w^T\boldsymbol{z}$,

$$\mathrm{kurt}(\boldsymbol{w}^T\boldsymbol{z}) = E[(\boldsymbol{w}^T\boldsymbol{z})^4] - 3\{E[(\boldsymbol{w}^T\boldsymbol{z})^2]\}^2. \tag{4}$$

A well-known algorism as FastICA tries to find $\boldsymbol{w}$ which maximize eq. (4) by iterative method. Requiring that the norm of $\boldsymbol{w}$ is unity, $||\boldsymbol{w}||^2 = 1$, (which makes $E[(\boldsymbol{w}^T\boldsymbol{z})^2] = ||\boldsymbol{w}||^2$). From the derivative of eq. (4), we get

$$\frac{\partial}{\partial \boldsymbol{w}_i}|\mathrm{kurt}(\boldsymbol{w}_i^T\boldsymbol{z})| = \begin{pmatrix} E[4(\boldsymbol{w}_i^T\boldsymbol{z})^3\boldsymbol{z}_1] \\ E[4(\boldsymbol{w}_i^T\boldsymbol{z})^3\boldsymbol{z}_2] \\ \vdots \end{pmatrix} - 12||\boldsymbol{w}_i||^2 \begin{pmatrix} w_{11} \\ w_{12} \\ \vdots \end{pmatrix}. \tag{5}$$

We, then, can find $\boldsymbol{w}_i$ as eq. (5) equals to zero by iterative method, that determines $s_i(t)$. Repeating the process of finding another component $\boldsymbol{w}_i$ as each $\boldsymbol{w}_i$ satisfies its orthogonality, we can identify all possible source signals $\tilde{\boldsymbol{s}}(t)$.

However, the method using kurtosis is sometimes quite sensitive to outliers. We also met this fact, and decided to use alternative FastICA as known to $g$-function method, which uses, instead of eq. (4),

$$\boldsymbol{w}_p = E[\boldsymbol{z}g(\boldsymbol{w}_p^T\boldsymbol{z})] - E[g'(\boldsymbol{w}_p^T\boldsymbol{z})]\boldsymbol{w}_p \tag{6}$$

where $g(y) = \tanh y$.

In summary, our procedure can be listed as follows.

1. Whiten the data $x(t)$ using power spectral density of each detector, and apply filtering if necessary.
2. Normalize $x(t)$ to $z(t)$ (mean zero, variance one).
3. Determine the number of independent components $m$. Set the counter $p$ to $p = 1$.
4. Randomly choose an initial weight matrix for $\boldsymbol{w}_p$.
5. Obtain $\boldsymbol{w}_p$ by eq. (6).
6. Orthogonalize $\boldsymbol{w}_p$ from other components:

$$\boldsymbol{w}_p = \boldsymbol{w}_p - \sum_{j=1}^{p-1}(\boldsymbol{w}_p^T\boldsymbol{w}_j)\boldsymbol{w}_j \tag{7}$$

7. Let $\boldsymbol{w}_p = \boldsymbol{w}_p/\|\boldsymbol{w}_p\|$

8. If $\boldsymbol{w}_p$ does not converge to the previous $\boldsymbol{w}_p$, then go back to 5.

9. Let $p = p + 1$. If $p \leq m$, go back to 4.

In order to confirm our converged $\boldsymbol{w}$ is unique, we repeated this sequence 5 times at least. In most cases, the converged solution was obtained directly.

Note that output signals from ICA do not have information of amplitude and signal's phase can be reversed, since we normalize the data first and the phase would be reversed due to the signature of $\det(\boldsymbol{w})$. We need further processes to identify them.

### B. Measure for identification of GW

For injection tests (Sec. III), we evaluate the output signal by comparing with the injected one, using its waveform and spectrum. When we test with an injection of inspiral wave signal, the waveform $h_{\rm insp}$ is

$$h_{\rm insp}(t; t_c, M_c) = A_{\rm insp} \left( \frac{5}{c(t_c - t)} \right)^{1/4} \times \sin \left\{ -2 \left( \frac{5GM_c}{c^3} \right)^{-5/8} (t_c - t)^{5/8} \right\} \quad (8)$$

where $c$, $G$, $M_c$, $t_c$ is the speed of light, the gravitation constant, the chirp mass, and the merger time, respectively. The factor of the amplitude $A_{\rm insp}$ can be written as $A_{\rm insp} = (1/r) \left( GM_c/c^2 \right)^{5/4}$, where $r$ is the distance to the source, but we just adjust $A_{\rm insp}$ as a parameter.

For real GW extraction (Sec. IV), we evaluate the output candidate signal, $\tilde{\boldsymbol{s}}_1(t)$, and the others, $\tilde{\boldsymbol{s}}_2(t)$ (, $\tilde{\boldsymbol{s}}_3(t)$), by defining the "strength of the extracted signal" using the area of the signal in the graph,

$$A_a = \sum_{t=t_s}^{t_c} \tilde{\boldsymbol{s}}_a(t) \cdot \Delta t \quad (9)$$

and calculate its ratio

$$\mathcal{A} = \frac{A_1}{A_2}, \text{ or } \mathcal{A} = \frac{2A_1}{A_2 + A_3}, \quad (10)$$

where $t_c$ is the time of coalescence and $t_s = t_c - 15$ ms for binary black-hole data. Large $\mathcal{A}$ suggests that $\tilde{\boldsymbol{s}}_1(t)$ has large amplitude than $\tilde{\boldsymbol{s}}_2(t)$ (and $\tilde{\boldsymbol{s}}_3(t)$ ).

We also compare the candidate signal $\tilde{\boldsymbol{s}}_1(t)$ and the estimated inspiral waveform using the chirp mass $M_c$ reported in GWOSC (Gravitational Wave Open Science Center) website [17], $h_{\rm insp}((t; t_c, M_c))$, by taking the residuals

$$\mathcal{R} = \sum_{t=t_s}^{t_c} |\tilde{\boldsymbol{s}}_1(t) - h_{\rm insp}(t; t_c, M_c)| \cdot \quad (11)$$

Small $\mathcal{R}$ event suggests better extraction than the other events.

### C. Finding the arrival time

One of the key procedures of our proposal is to find the arrival time of GW signal to each detector by shifting input data continually. For normal applications of ICA method, we have not seen such an implementation, but it is necessary for GW signals.

In this article, we only demonstrate the applications for the known events up to O3, so the merger time, $t_c$, is took as a given suggested value. We then search GW signal around $t_c$ by shifting the data from each detector up to $\pm 30$ ms ($\sim$ distance between Hanford and Virgo), and search the combination which shows the largest $\mathcal{A}$. As we show later in Table III, the result of the shifted-time, e.g. $\Delta t_{\rm HL} (= t_{\rm L} - t_{\rm H})$ between Hanford and Livingston, can be identified with the difference of the arrival time of GW, and its comparison with those in published articles will also support how our method works.

## III. DEMONSTRATIONS WITH INJECTED GW SIGNALS

In this section, we discuss how ICA works for extracting GW with test problems. The target discussion is at what level we can apply ICA for signal extraction, i.e. applicable characteristics of signals.

### A. Injections of inspiral signal to Gaussian Noise

The first test is an injection of inspiral wave signal to Gaussian noise.

We prepare two different Gaussian-type noises, $n_{1\rm G}$ and $n_{2\rm G}$, and inject $h_{\rm insp}$ to them as

$$\text{Model 1 : } \begin{cases} x_1(t) = n_{1\rm G}(t) + h_{\rm insp}(t; t_c, M_c), \\ x_2(t) = n_{2\rm G}(t) + h_{\rm insp}(t; t_c, M_c). \end{cases} \quad (12)$$

If we put the same Gaussian noise for both $x_1(t)$ and $x_2(t)$, then the test is the same with well-known blind signal separation problem. Model 1 is different from this, so somewhat challenging for the cases of weak injected signal.

TABLE I. Results of Model 1 [injection of inspiral wave to the Gaussian noise]: the fitting parameter $\alpha$ and $\beta$ of the Fourier spectrum of the extracted signal. Note that $\alpha = 15.3$ and $\beta = 0.63$ for the injected signal.

| $\lvert h_{\rm insp} \rvert$ | $\alpha$ | $\beta$ | ref. |
|---|---|---|---|
| [1.0, 5.0] | 13.7 | 0.665 | Fig.1(a4) |
| [0.5, 2.5] | 7.53 | 0.706 | Fig.1(b4) |
| [0.2, 1.0] | -57.5 | 0.661 | Fig.1(c4) |

Figure 1 shows examples of the results of this model. The length of the data is one second, $t = [0, 1]$, with its sampling rate 4096. We set the merger time at $t_c = 1.0 + 1/4096$. We used the chirp mass $M_c =$

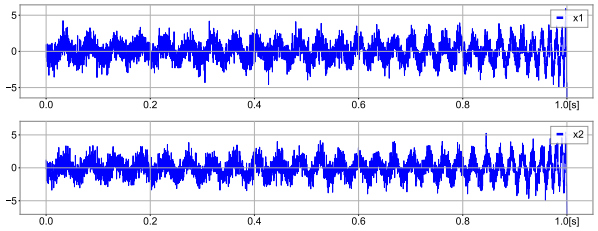


(a1) Input signals with $|h_{\rm insp}(t=1)|/\overline{|n_{\rm G}(t)|} = 5.0$.

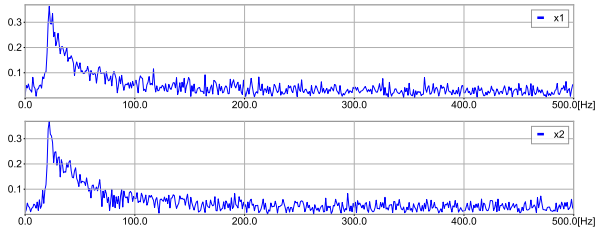


(a2) Fourier spectrum of (a1).

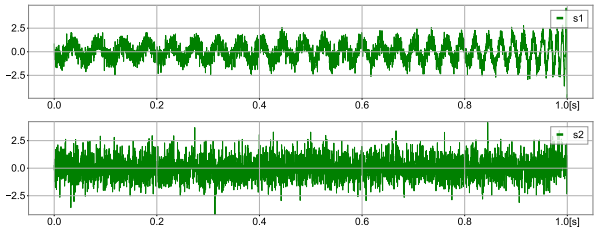


(a3) Output of ICA for (a1).


(a4) Fourier spectrum of (a3).

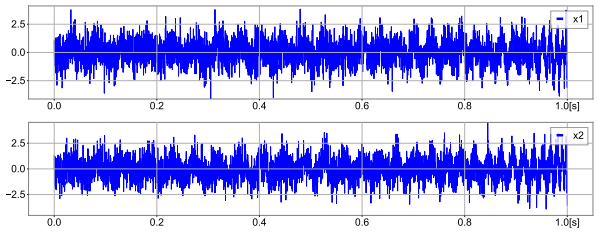


(b1) Input signals with $|h_{\rm insp}(t=1)|/\overline{|n_{\rm G}(t)|} = 2.5$.

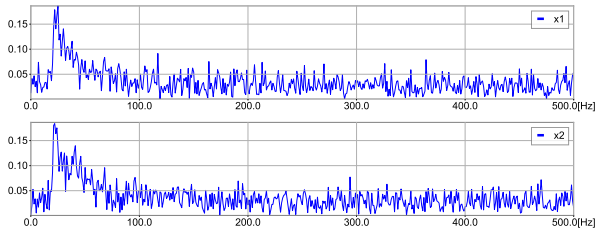


(b2) Fourier spectrum of (b1).

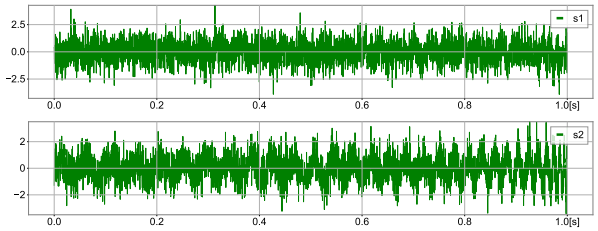


(b3) Output of ICA for (b1).

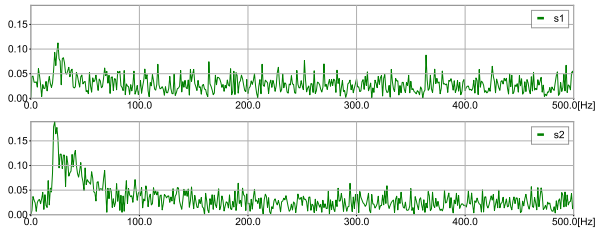


(b4) Fourier spectrum of (b3).

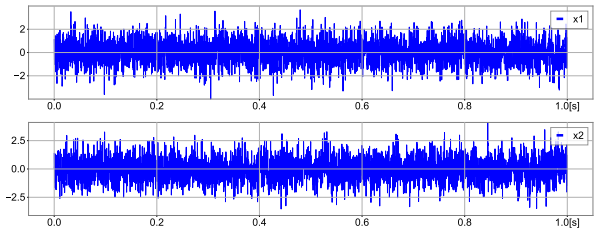


(c1) Input signals with $|h_{\rm insp}(t=1)|/\overline{|n_{\rm G}(t)|} = 1.0$.

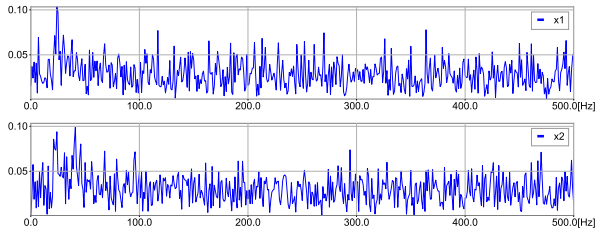


(c2) Fourier spectrum of (c1).

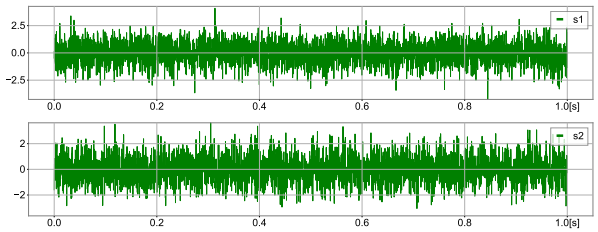


(c3) Output of ICA for (c1).

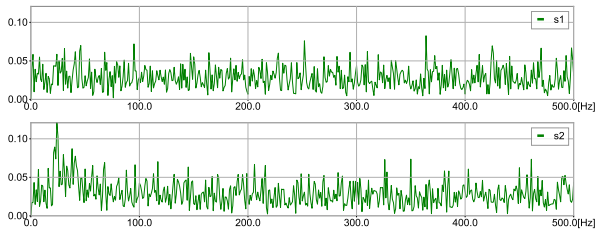


(c4) Fourier spectrum of (c3).

FIG. 1. An example of GW extraction using ICA, the case of Model 1 [eq. (12)], injection of an inspiral wave to Gaussian background. Figures are of $|h_{\rm insp}(t=1)|/\overline{|n_{\rm G}(t)|} = 5.0$ (a1-a4), 2.5 (b1-b4) and 1.0 (c1-c4). We use one-second length data $t = [0, 1]$, with $t_c = 1 + 1/4096$. We see inspiral wave is clearly extracted for (a), but not for (c).

$26.12M_\odot$, which is of $30M_\odot$-$30M_\odot$ binary at the observed frame. We measure the amplitude of injected inspiral signal by the averaged amplitude of the noises, $\overline{|n_{1\rm G}|^2} = \overline{|n_{2\rm G}|^2} = 1$. We show three cases for the injected inspiral signals which evolve $|h_{\rm insp}| = [1.0, 5.0], [0.5, 2.5]$, and $[0.2, 1.0]$ for $t = [0, 1]$ as shown in Fig. 1 (a1), (b1) and (c1), respectively. We see the inspiral characteristics is observable by eyes over 30 Hz in Fig. 1 (a1).

In Fig. 1, we show also their Fourier spectrum in (a2), (b2), and (c2), and the output results of ICA in (a3), (b3), and (c3) together with these Fourier spectrum in (a4), (b4), and (c4). Remark that the results of ICA do not include the information of its strongness of each mode, i.e. the amplitude of output data do not indicate their strongness in the input data.

In order to see how the extracted signal matches with the injected one, we approximate the power spectrum of the output signal [Fig.1(a4), (b4), and (c4)] with a function $(f-\alpha)^{-\beta}$ for $f = [20, 300]$ Hz where $\alpha, \beta$ are constants, and compared them with those of the injected signal, $(f-15.3)^{-0.63}$. We show the comparison in Table I. We made the same extractions 10 times by changing the initial guess of $\boldsymbol{w}_p$ randomly, and show the average of the fitting parameter $\alpha, \beta$ in the table. As expected, if the amplitude of injected signals is large, then ICA clearly identifies the signal. We see the identification is hard when the amplitude of injected signal is as the same level of the noise.

### B. Injections of GW signal to real detector data

We next demonstrate signal extractions of injected waves from the real detector data. We use the detector data around GW150914 (GPS time of $t_c = 1126259462.4$) of LIGO-Hanford, $n_{\rm H}(t)$, and of LIGO-Livingston, $n_{\rm L}(t)$, which we downloaded from GWOSC.

We made two tests. One is the injection of a sinusoidal wave,

$$\text{Model 2}: \begin{cases} x_1(t) = n_{\rm H}(t) + \sin(2\pi f t), \\ x_2(t) = n_{\rm L}(t) + \sin(2\pi f t) \end{cases} \tag{13}$$

and the other is an inspiral wave [eq.(8)],

$$\text{Model 3}: \begin{cases} s_1(t) = n_{\rm H}(t) + h_{\rm insp}(t; t_0, M_c), \\ s_2(t) = n_{\rm L}(t) + h_{\rm insp}(t; t_0, M_c). \end{cases} \tag{14}$$

For Model 2, we used two second data around the merger time of GW150914, and we set $f = 213$ Hz which is independent from the known line noises. Figure 2 and Table II are the results of Model 2. By changing the amplitude, we show the cases of signal-to-noise ratio (SNR) 20 (Fig.(a)), 10 (b) and 5 (c). Figures (a1), (b1) and (c1) are input data of $x_1(t)$ and $x_2(t)$, where we show only the center one-second length. Figures (a2), (b2) and (c2) are the Fourier spectrum of (a1), (b1) and (c1) respectively. We see the original detector data include line noise at 60 Hz and 120 Hz. Figures (a3), (b3), and (c3) are the output of ICA, and (a4), (b4), (c4) are their Fourier spectrum, respectively. In order to judge whether ICA extracted the injected wave, we show in Table II the ratio of the power spectrum of 213 Hz over those of the average of 150-250 Hz. We think we are safe to say the extraction was effective for the cases SNR $\geq 10$.

For Model 3, we used one second data before one second of the merger time $t_c$ of GW150914. The injected inspiral wave is $h(t; t_c - 1\ {\rm s}, 26M_\odot)$. Results are shown in Figure 3 with the same notation with previous figures. Note that we filtered for $f > 300$ Hz and also that the input data has strong line noise at 60 Hz. The SNR of the injected signal is 20.9 (a1-a4), 16.8 (b1-b4), and 10.5 (c1-c4). We see the inspiral feature in Fourier spectrum of the output data for SNR $> 15$.

TABLE II. Results of Model 2 [injection of sinusoidal wave to the real detector data]: SNR and excess power spectrum of 213 Hz in the extracted data over the average of 150-2050 Hz.

| SNR to $h_H$ | SNR to $h_L$ | excess power | ref. |
|---|---|---|---|
| 20.8 | 20.0 | 7.78 | Fig.2(a4) |
| 10.4 | 10.0 | 3.76 | Fig.2(b4) |
| 5.2 | 5.0 | 1.93 | Fig.2(c4) |

## IV. APPLICATIONS TO REAL GW EXTRACTIONS

In this section, we demonstrate GW extractions of the real events.

### A. GW150914

We show the case of GW150914[1] a bit detail. This is the first detection of GW, and is well-tested in various ways as the standard one. The event was observed by Hanford (H) and Livingston (L) observatories, and the announced network-SNR in GWOSC is 26.0.

We used one-second data around $t_c$ with its sampling-rate 4096. As a pre-process, we whitened the data using each detector's power spectral density, and also filtered the data to [20, 300] Hz. By shifting Livingston's data with every 1/4096 sec, we applied ICA with 5 different initial weight matrix $\boldsymbol{w}_p$ and searched the data set which shows the maximum strength of the extracted signal, $\mathcal{A}$ [eq. (10)]. The calculations requires only 90 s by a laptop for finding the best $\mathcal{A}$ result.

We found the maximum $\mathcal{A}$ when $\Delta t_{\rm HL} = -7.32$ ms. Figure 5 shows $\mathcal{A}$ as a function of $\Delta t_{\rm HL}$. The plot includes the results of our 5 different initial weight matrix $\boldsymbol{w}_p$, and we see the maximum of $\mathcal{A}$ is independent from those initial value (which means $\boldsymbol{w}_p$ is well-converged for each cases). From Figure 5, we estimate $\Delta t_{\rm HL}$ with the error-bar $\pm 0.15$ ms. Note that the LIGO-Virgo paper [1]

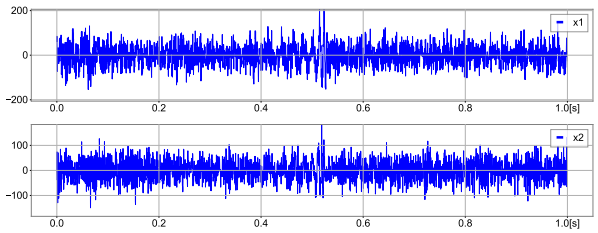


(a1) Input signals of SNR 20.

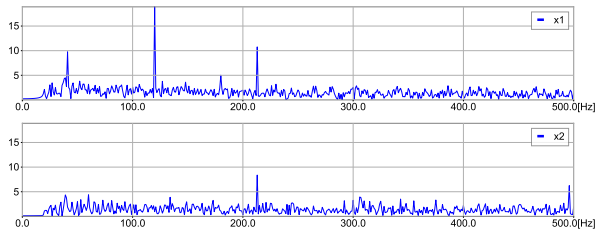


(a2) Fourier spectrum of (a1).

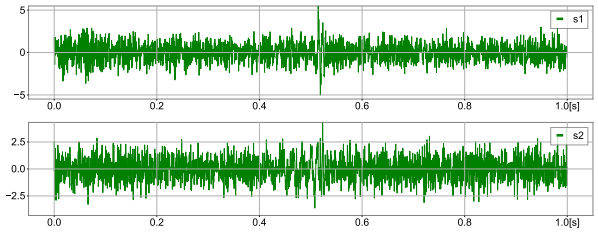


(a3) Output of ICA for (a1).


(a4) Fourier spectrum of (a3).

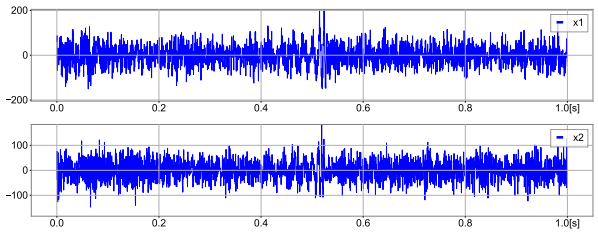


(b1) Input signals of SNR 10.

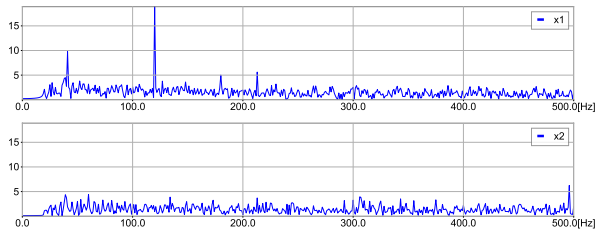


(b2) Fourier spectrum of (b1).

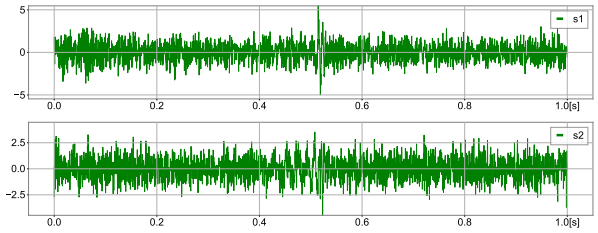


(b3) Output of ICA for (b1).

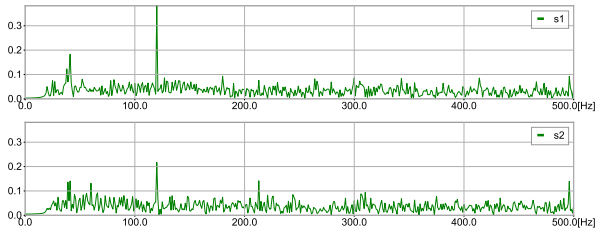


(b4) Fourier spectrum of (b3).

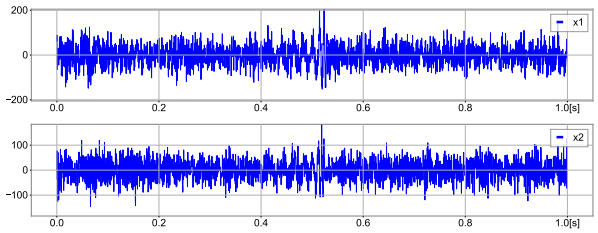


(c1) Input signals of SNR 5.

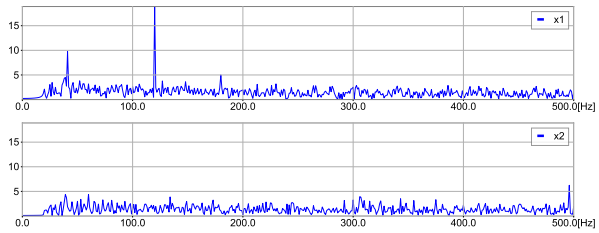


(c2) Fourier spectrum of (c1).

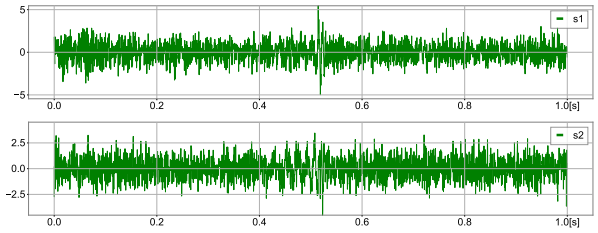


(c3) Output of ICA for (c1).


(c4) Fourier spectrum of (c3).

FIG. 2. An example of GW extraction using ICA, the case of Model 2 [eq. (13)], injections of a sinusoidal wave of 213 Hz to the Hanford and Livingston data around the event GW190914. (Note that the original data include large noises at 60 Hz and 120 Hz.) The signal-to-noise ratio (SNR) is 20 (a1-a4), 10 (b1-b4), and 5 (c1-c4). We see the injected wave is clearly extracted for (a) and (b), but not for (c).

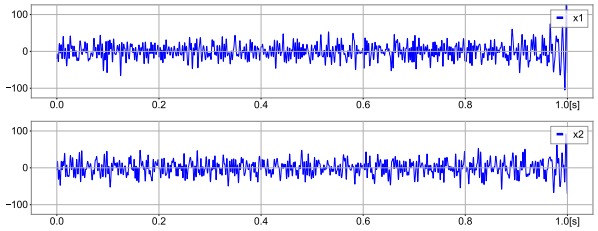


(a1) Input signals of SNR 20.9.

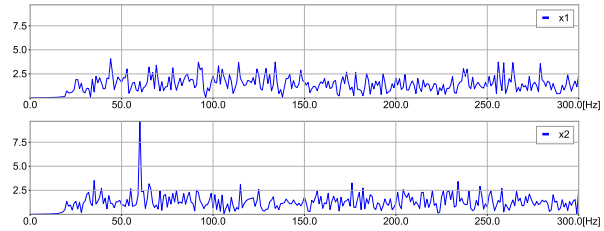


(a2) Fourier spectrum of (a1).

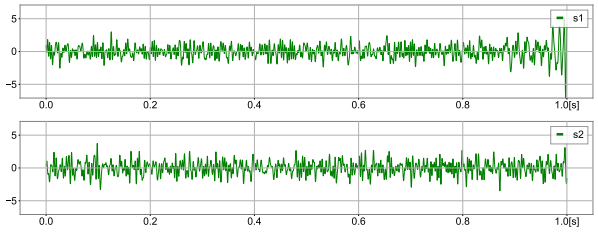


(a3) Output of ICA for (a1).


(a4) Fourier spectrum of (a3).

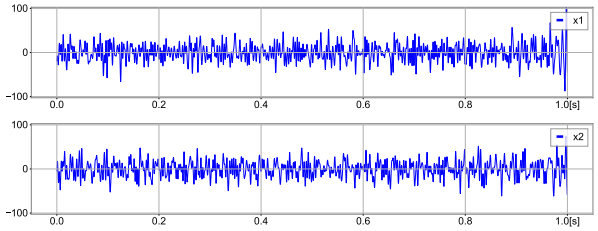


(b1) Input signals of SNR 16.8.

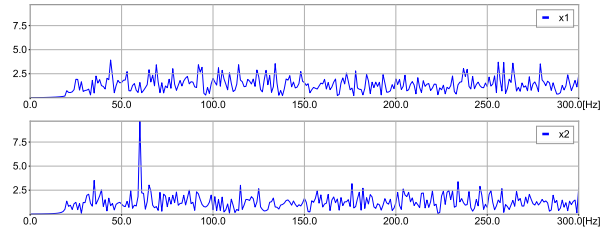


(b2) Fourier spectrum of (b1).

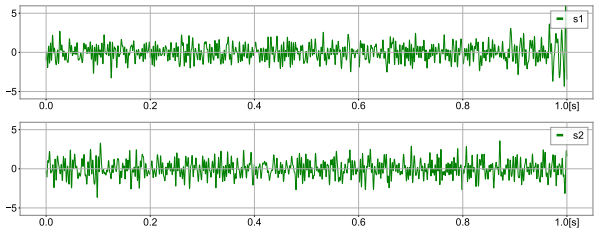


(b3) Output of ICA for (b1).

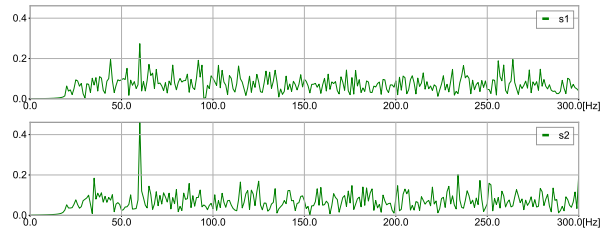


(b4) Fourier spectrum of (b3).

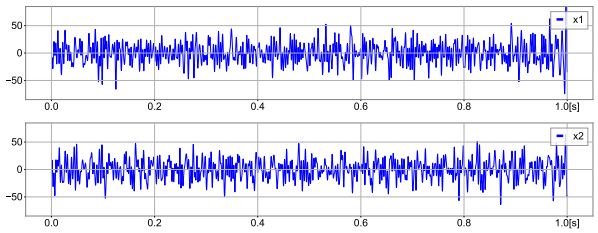


(c1) Input signals of SNR 10.5.

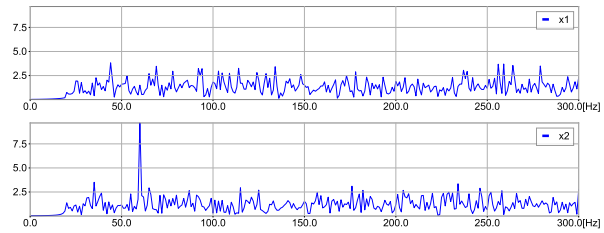


(c2) Fourier spectrum of (c1)

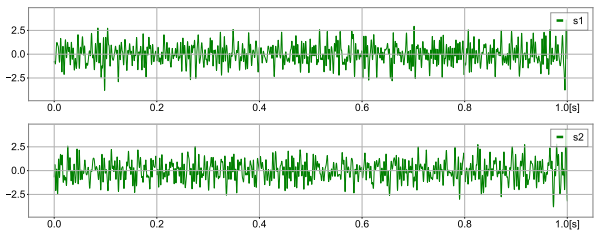


(c3) Output of ICA for (c1).

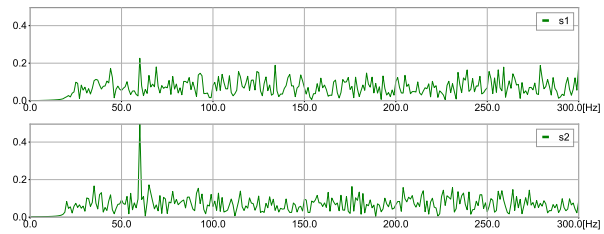


(c4) Fourier spectrum of (c3).

FIG. 3. Test of GW extraction using ICA: the case of Model 3 [eq. (14)], injections of a inspiral wave signal to the Hanford and Livingston data one second before the event GW150914. The SNR of the injected signal is 20.9 (a1-a4), 16.8 (b1-b4), and 10.5 (c1-c4). We see the inspiral feature in Fourier spectrum of the output data for SNR $> 15$. Note that we filtered for $f > 300$ Hz and also that the input data has strong line noise at 60 Hz.

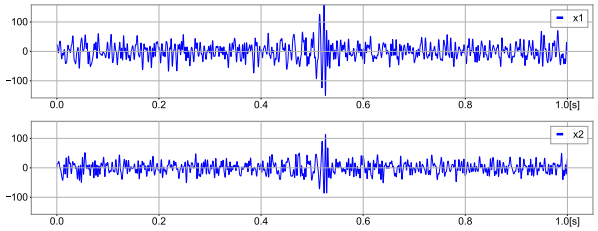


(a) Input signals with $\Delta t_{\rm HL} = -7.32$ ms. The data x1 and x2 are of Hanford and Livingston data, respectively.

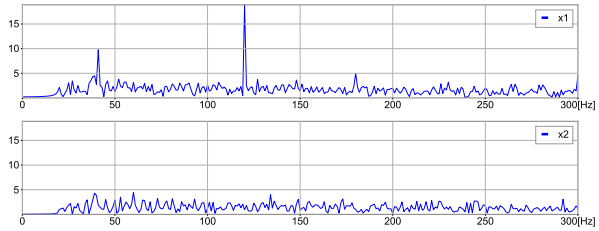


(b) Fourier spectrum of (a).

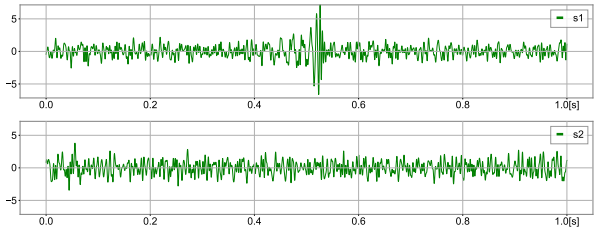


(c) Output of ICA.

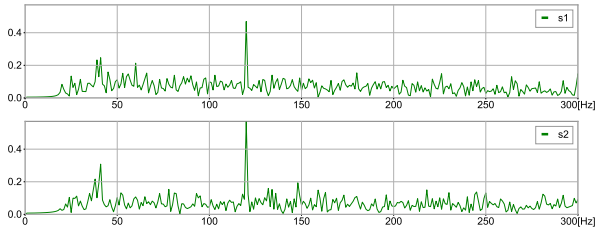


(d) Fourier spectrum of (c).

FIG. 4. Application to GW150914. (a/b) The set of input data and its spectrum with $\Delta t_{\rm HL} = -7.32$ ms which shows the largest $\mathcal{A}$ in the output of ICA. The x1 and x2 indicates the data of Hanford and Livingston, respectively. (c/d) The output of ICA, and its spectrum. We clearly see the signal (s1) is separted from the other (s2). Note that the input data have a line noise at 120 Hz.

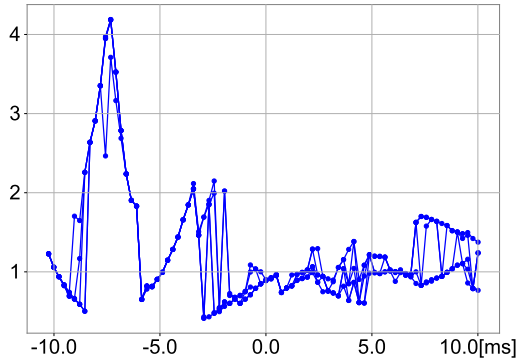


FIG. 5. The strength of the extracted signal, $\mathcal{A}$ [eq. (10)] as a function of $\Delta t_{\rm HL}$ for the case of GW150914. Five trials of different initial weight matrix are plotted at each $\Delta t_{\rm HL}$. We see the maximum is at $\Delta t_{\rm HL} = -7.32^{+0.15}_{-0.15}$ ms. Note that LIGO-Virgo paper [1] shows $\Delta t_{\rm HL} = -6.9^{+0.5}_{-0.4}$ ms.

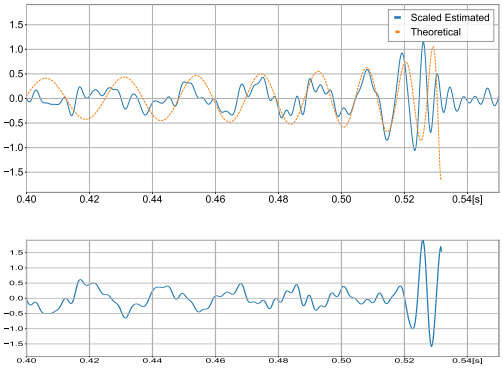


FIG. 6. Extraction of GW150914. (Upper) The output data (Fig. 4 (c) s1) is overlapped with $h_{\rm insp}(t; t_c, M_c = 30.8 M_\odot)$. (Lower) The residuals.

denotes $\Delta t_{\rm HL} = -6.9^{+0.5}_{-0.4}$ ms. Our number is consistent with [1] and with a small error-bar.

We plot the input data (x1, x2) and the output data (s1, s2) for the largest $\mathcal{A}$ case in Fig. 4. For the output data s1 [in Fig. 4(c)], we next searched the best matched inspiral waveform, $h_{\rm insp}(t; t_c, M_c)$, by changing $M_c$ and amplitude, measuring its residuals, $\mathcal{R}$. We found $M_c = 30.8 M_\odot$ shows the lowest residuals. This case is shown as Fig. 6, and we see how the output s1 is similar to the expected inspiral signal.

GWOSC webpage shows $M_c = 28.6^{+1.7}_{-1.5} M_\odot$ as an estimated value in the source frame. Our $M_c$ is in the observed frame, which differs as

$$M_c^{\rm obs} = M_c^{\rm source}(1+z) \tag{15}$$

where $z$ is the redshift parameter of the source. From error-bars in $M_c^{\rm source}$ in GWOSC data, we calculate $z$ (hereafter we denote $z_{\rm ICA}$) as $z_{\rm ICA} = 0.077 \pm 0.06$. The redshift $z$ of GW150914 in GWOSC webpage is $z = 0.09 \pm 0.03$. Therefore our result is again consistent with them.

TABLE III. Results of the wave extractions by ICA for large SNR events in O1-O3. The column obs shows which detector (Hanford/Livingston/Virgo) observed. SNR is the network signal-to-noise ratio (centered value) which is announced in GWOSC (https://gwosc.org). $\Delta t_{\rm HL}$ is the time shift between Hanford data and Livingston data, $t_{\rm L} - t_{\rm H}$, in ms when ICA shows the best separation of the signal. $\mathcal{A}$ is the ratio of extracted signal to the other noise(s) evaluated by eq. (10). $\mathcal{R}$ is the residuals of the extracted waveform and estimated inspiral waveform, (11), between $[t_c - 0.15$ ms, $t_c]$. See table IV for comparisons of chirp-mass and red-shift.

| event | obs | SNR | $\Delta t_{\rm HL}$ (ms) | $\Delta t_{\rm HV}$ (ms) | $\Delta t_{\rm LV}$ (ms) | $\mathcal{A}$ | $\mathcal{R}/10^{-12}$ | ref. |
|---|---|---|---|---|---|---|---|---|
| GW150914 | HL | 26.0 | $-7.32\pm^{1.5}_{1.5}$ | – | – | 4.19 | 5.88 | Fig.4 |
| GW190521_074359 | HL | 32.8 | $-6.35\pm^{0.98}_{0.49}$ | – | – | 1.83 | 10.3 | Fig.7(a) |
| GW191109_010717 | HL | 47.5 | $3.17\pm^{0.98}_{0.73}$ | – | – | 3.40 | 18.4 | Fig.7(b) |
| GW191204_171526 | HL | 8.55 | $-2.44\pm^{0.49}_{0.73}$ | – | – | 2.07 | 3.27 | Fig.7(c) |
| GW191216_213338 | HV | 8.33 | – | $-11.0\pm^{1.5}_{0.73}$ | – | 3.08 | 2.09 | Fig.7(d) |
| GW200112_155838 | LV | 27.4 | – | – | $-23.2\pm^{0.49}_{0.24}$ | 2.43 | 10.5 | Fig.7(e) |
| GW170814 | HLV | 24.1 | $-8.06\pm^{0.49}_{0.98}$ | $0.98\pm^{2.4}_{0.24}$ | – | 3.54 | 5.07 | Fig.7(f) |
| GW190412 | HLV | 13.3 | $-3.91\pm^{0.24}_{0.24}$ | $-13.92\pm^{0.98}_{0.49}$ | – | 2.21 | 4.40 | Fig.7(g) |
| GW190521 | HLV | 63.3 | $2.93\pm^{0.49}_{1.2}$ | $-25.15\pm^{0.49}_{1.7}$ | – | 2.85 | 31.8 | Fig.7(h) |
| GW190814 | HLV | 6.11 | $2.20\pm^{0.49}_{0.24}$ | $21.24\pm^{0.73}_{0.24}$ | – | 2.00 | 1.65 | Fig.7(i) |
| GW200129_065458 | HLV | 27.2 | $3.42\pm^{0.98}_{0.24}$ | $-18.31\pm^{0.24}_{0.24}$ | – | 3.96 | 11.3 | Fig.7(j) |
| GW200224_222234 | HLV | 31.1 | $-3.66\pm^{2.7}_{0.24}$ | $-9.28\pm^{0.24}_{0.98}$ | – | 3.28 | 13.4 | Fig.7(k) |
| GW200311_115853 | HLV | 26.6 | $-3.66\pm^{0.73}_{1.2}$ | $-27.10\pm^{2.2}_{2.2}$ | – | 3.17 | 4.34 | Fig.7(l) |

TABLE IV. Comparisons of chirp mass, $M_c^{\rm source}$, shown in GWOSC and the one obtained by ICA,$M_c^{\rm obs}$ from the best fit inspiral-wave model. The difference can be regard as redshift factor $(1 + z_{\rm ICA})$. The redshift factor in GWOSC, $z$, is also shown.

| | | | GWOSC | | ICA | | |
|---|---|---|---|---|---|---|---|
| event | obs | SNR | $M_c^{\rm source}/M_\odot$ | $z$ | $M_c^{\rm obs}/M_\odot$ | $z_{\rm ICA}$ | ref. |
| GW150914 | HL | 26.0 | $28.6^{+1.7}_{-1.5}$ | $0.09^{+0.03}_{-0.03}$ | 30.8 | $0.077^{+0.06}_{-0.06}$ | Fig.4 |
| GW190521_074359 | HL | 25.9 | $32.8^{+3.2}_{-2.8}$ | $0.21^{+0.10}_{-0.10}$ | 36.4 | $0.11^{+0.10}_{-0.10}$ | Fig.7(a) |
| GW191109_010717 | HL | 17.3 | $47.5^{+9.6}_{-7.5}$ | $0.25^{+0.18}_{-0.12}$ | 53.7 | $0.13^{+0.22}_{-0.19}$ | Fig.7(b) |
| GW191204_171526 | HL | 17.5 | $8.56^{+0.41}_{-0.28}$ | $0.34^{+0.25}_{-0.18}$ | 11.1 | $0.29^{+0.04}_{-0.06}$ | Fig.7(c) |
| GW191216_213338 | HV | 18.6 | $8.33^{+0.22}_{-0.19}$ | $0.07^{+0.02}_{-0.03}$ | 9.00 | $0.08^{+0.03}_{-0.03}$ | Fig.7(d) |
| GW200112_155838 | LV | 19.8 | $27.4^{+2.6}_{-2.1}$ | $0.24^{+0.07}_{-0.08}$ | 32.7 | $0.19^{+0.10}_{-0.10}$ | Fig.7(e) |
| GW170814 | HLV | 17.7 | $24.1^{+1.4}_{-1.1}$ | $0.12^{+0.03}_{-0.04}$ | 26.0 | $0.08^{+0.05}_{-0.06}$ | Fig.7(f) |
| GW190412 | HLV | 19.8 | $13.3^{+0.5}_{-0.5}$ | $0.15^{+0.04}_{-0.04}$ | 14.8 | $0.11^{+0.04}_{-0.04}$ | Fig.7(g) |
| GW190521 | HLV | 14.3 | $63.3^{+19.6}_{-14.6}$ | $0.56^{+0.36}_{-0.27}$ | 81.7 | $0.29^{+0.39}_{-0.30}$ | Fig.7(h) |
| GW190814 | HLV | 25.3 | $6.11^{+0.06}_{-0.05}$ | $0.05^{+0.01}_{-0.01}$ | 6.35 | $0.04^{+0.01}_{-0.01}$ | Fig.7(i) |
| GW200129_065458 | HLV | 26.8 | $27.2^{+2.1}_{-2.3}$ | $0.18^{+0.05}_{-0.07}$ | 30.6 | $0.13^{+0.10}_{-0.08}$ | Fig.7(j) |
| GW200224_222234 | HLV | 20.0 | $31.1^{+3.3}_{-2.7}$ | $0.32^{+0.08}_{-0.11}$ | 37.6 | $0.21^{+0.11}_{-0.12}$ | Fig.7(k) |
| GW200311_115853 | HLV | 17.8 | $26.6^{+2.4}_{-2.0}$ | $0.23^{+0.05}_{-0.07}$ | 31.0 | $0.17^{+0.09}_{-0.10}$ | Fig.7(l) |

### B. Other events

We continue the similar analysis for other GW events from binary BHs with higher SNR events in O1-O3. Figs. 7 show the input data (x1, x2, x3) and the output data (s1, s2, s3) which show the largest $\mathcal{A}$. For three-detector events, we made 2-dimensional search for shifting data, which requires 20100 combinations at maximum, and the computation time is around 20 hours. The results of ICA are summarized in Table III and IV.

Table III can be used for understanding how ICA works. Roughly summarizing, the parameter $\mathcal{A}$, which is a measure of the quality of extraction, is almost the same regardless of the SNR. The residual $\mathcal{R}$, which is a measure of how the extracted wave can be matched with inspiral waveform, has negative correlation with SNR.

Table IV can be used for understanding how the results of ICA are realistic. By making the matches with inspiral wave, we can specify $M_c^{\rm obs}$ for each event. With $M_c^{\rm source}$ in GWOSC table, we compare the redshift parameters in GWOSC table and $z_{\rm ICA}$. As we see in the table IV, all $z$ parameters are consistent.

## V. SUMMARY

We applied independent component analysis (ICA) to extract gravitational-wave signals. From injection tests, we see that the extractions are available even from the real interferometer data if the signals' strength (SNR) is 15 or higher. We then demonstrate this method to the inspiral-wave extraction for binary black-hole events, especially 13 high-SNR events up to O3 (GWTC-3 catalog). As we show in Table III the extractions are per-

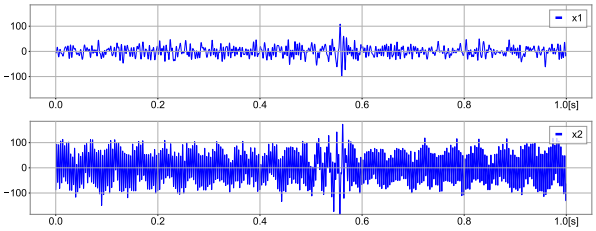


(a1) Input signals of GW190521_074359 with $\Delta t_{\rm HL} = -6.35$ ms. The data x1 and x2 are of Hanford and Livingston data, respectively.

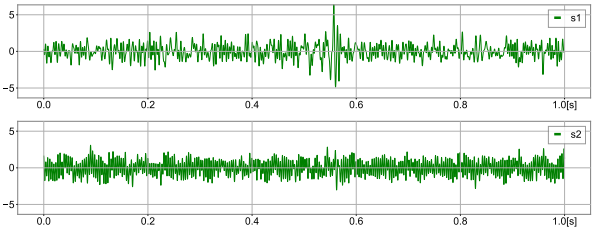


(a2) Output of ICA for GW190521_074359.

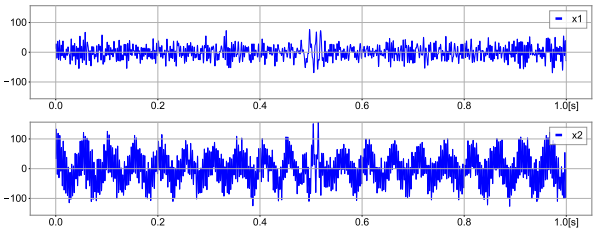


(b1) Input signals of GW191109_010717 with $\Delta t_{\rm HL} = +3.17$ ms. The data x1 and x2 are of Hanford and Livingston data, respectively.

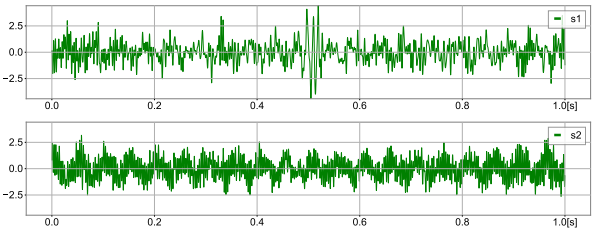


(b2) Output of ICA for GW191109_010717.

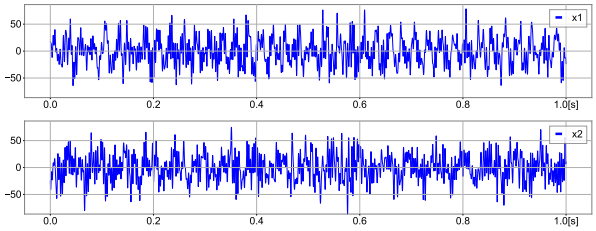


(c1) Input signals of GW191204_171526 with $\Delta t_{\rm HL} = -2.44$ ms. The data x1 and x2 are of Hanford and Livingston data, respectively.

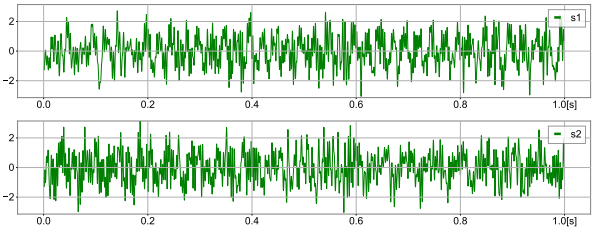


(c2) Output of ICA for GW191204_171526.

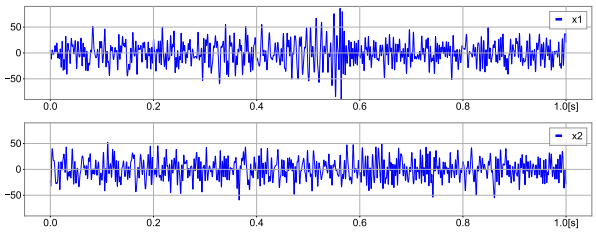


(d1) Input signals of GW191216_213338 with $\Delta t_{\rm HV} = -11.0$ ms. The data x1 and x2 are of Hanford and Virgo data, respectively.

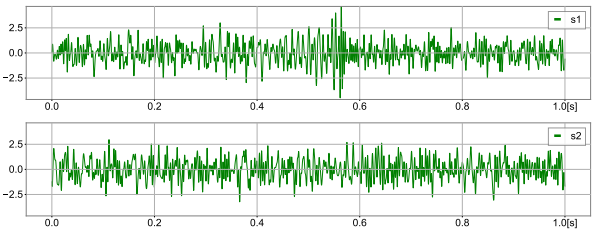


(d2) Output of ICA for GW191216_213338

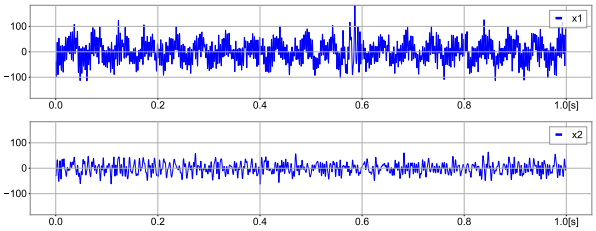


(e1) Input signals of GW200112_155838 with $\Delta t_{\rm LV} = -23.2$ ms. The data x1 and x2 are of Livingston and Virgo data, respectively.

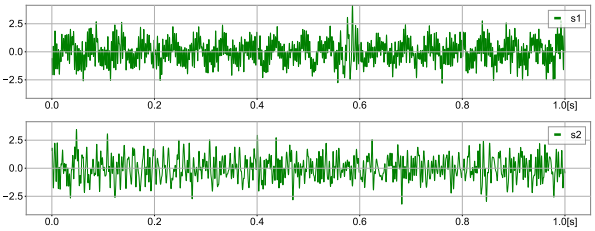


(e2) Output of ICA for GW200112_155838.

FIG. 7. Input and Output data of ICA analysis.

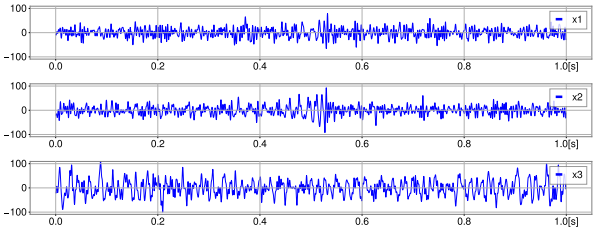


(f1) Input signals of GW170814 with $\Delta t_{\rm HL} = -8.06$ ms and $\Delta t_{\rm HV} = +0.98$ ms. The data x1, x2, and x3 are of Hanford, Livingston, and Virgo, respectively.

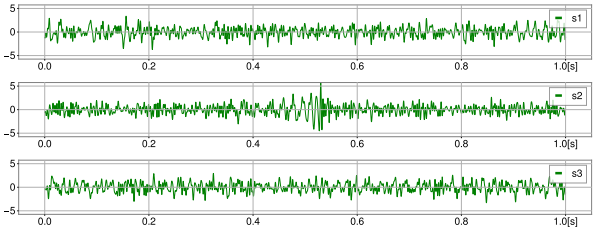


(f2) Output of ICA for GW170814.

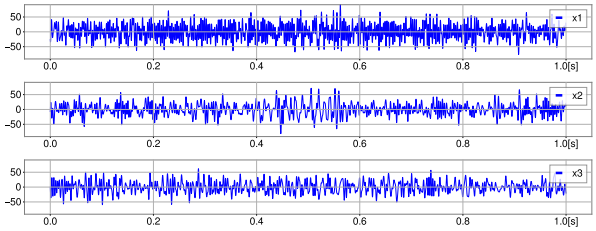


(g1) Input signals of GW190412 with $\Delta t_{\rm HL} = -3.91$ ms and $\Delta t_{\rm HV} = -13.92$ ms. The data x1, x2, and x3 are of Hanford, Livingston, and Virgo, respectively.

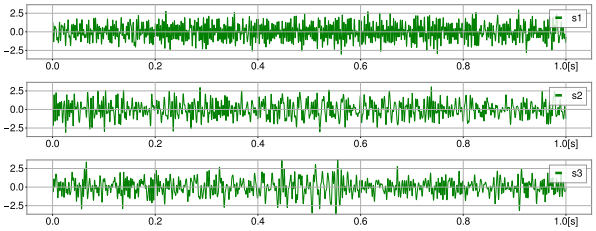


(g2) Output of ICA for GW190412.

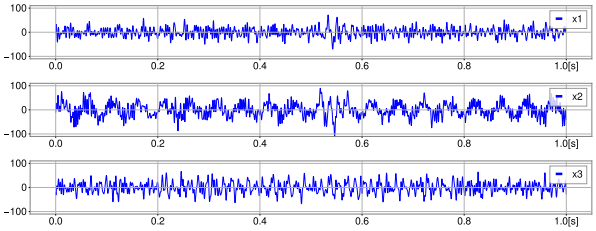


(h1) Input signals of GW190521 with $\Delta t_{\rm HL} = +2.93$ ms and $\Delta t_{\rm HV} = -25.15$ ms. The data x1, x2, and x3 are of Hanford, Livingston, and Virgo, respectively.

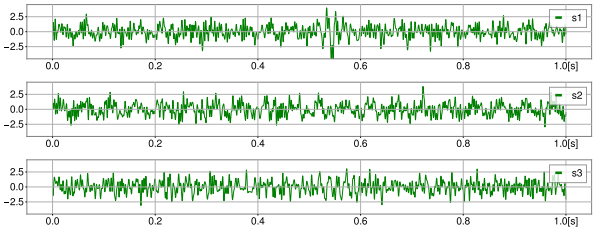


(h2) Output of ICA for GW190521.

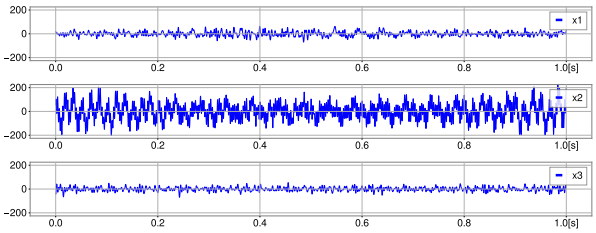


(i1) Input signals of GW190814 with $\Delta t_{\rm HL} = +2.20$ ms and $\Delta t_{\rm HV} = +21.24$ ms. The data x1, x2, and x3 are of Hanford, Livingston, and Virgo, respectively.

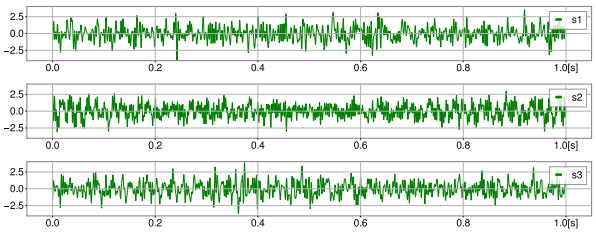


(i2) Output of ICA for GW190814.

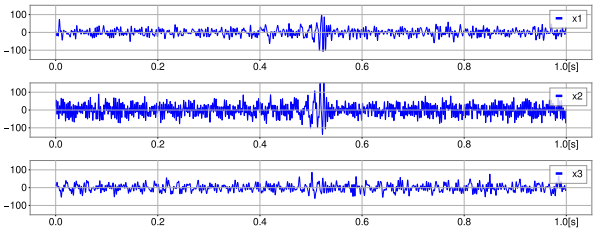


(j1) Input signals of GW200129_065458 with $\Delta t_{\rm HL} = +3.42$ ms and $\Delta t_{\rm HV} = -18.31$ ms. The data x1, x2, and x3 are of Hanford, Livingston, and Virgo, respectively.

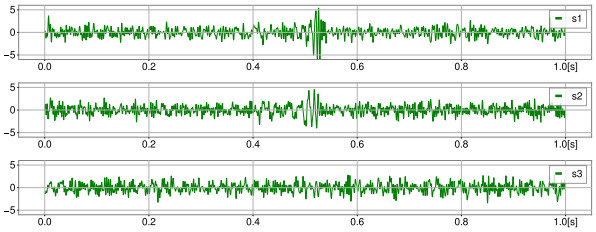


(j2) Output of ICA for GW200129_065458.

FIG. 7. Input and Output data of ICA analysis (cont.)

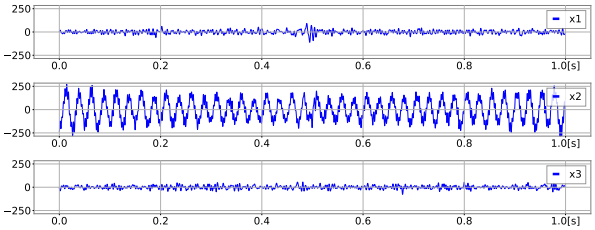


(k1) Input signals of GW200224_222234 with $\Delta t_{\rm HL} = -3.66$ ms and $\Delta t_{\rm HV} = -9.28$ ms. The data x1, x2, and x3 are of Hanford, Livingston, and Virgo, respectively.

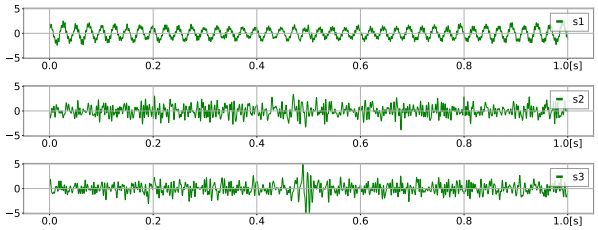


(k2) Output of ICA for GW200224_222234.

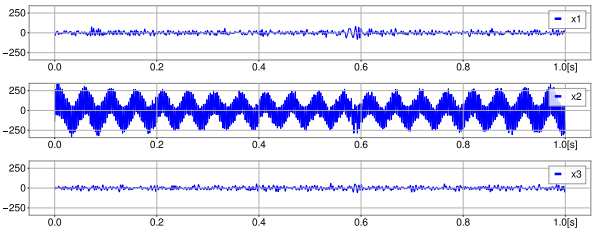


(l1) Input signals of GW200311_115853 with $\Delta t_{\rm HL} = -3.66$ ms and $\Delta t_{\rm HV} = -27.10$ ms. The data x1, x2, and x3 are of Hanford, Livingston, and Virgo, respectively.

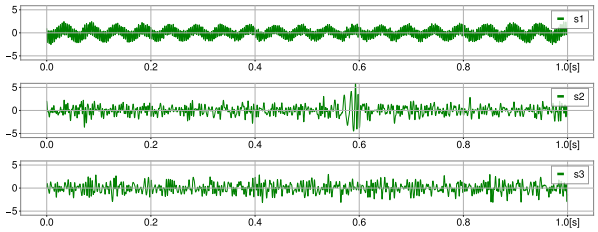


(l2) Output of ICA for GW200311_115853.

FIG. 7. Input and Output data of ICA analysis (cont.)

formed for all events, and as we show in Table IV, the fitted waveforms show consistent parameters $M_c$ and $z$ with those reported by LIGO-Virgo-KAGRA collaboration papers.

We remark again that ICA is based on the idea how the signal is mathematically independent from others. The only non-Gaussian waves can be extracted. Additionally, the current FastICA method starts from normalizing and whitening the input data, which makes the output signals without information of the amplitude, and the phase can be reversed. If we know the waveform like our applications to GWTC-3, we would determine the phase by evaluating the residual, while the amplitude itself remain undetermined.

Although there are limitations, the method proposed here is attractive because it does not use any templates in advance. If we could visualize the waveforms first, it would undoubtedly help theoretical understanding. We think this ICA approach will contribute for testing GR and also for finding unknown GW signals.

We thank Hirotaka Yuzurihara for his suggestion on a technical procedure. This work was supported by JSPS KAKENHI Grants No. 24K07029 and 18K03630.

[1] B. P. Abbott et al. (LIGO Scientific Collaboration and Virgo Collaboration), Phys. Rev. Lett. **116**, 061102 (2016).
[2] B. P. Abbott et al. (LIGO Scientific Collaboration and Virgo Collaboration), Phys. Rev. Lett. **119**, 161101 (2017).
[3] R. Abbott et al. (LIGO Scientific Collaboration, Virgo Collaboration, and KAGRA Collaboration) Phys. Rev. X **13**, 041039 (2023).
[4] R. Abbott et al. (LIGO Scientific Collaboration, Virgo Collaboration, and KAGRA Collaboration) Phys. Rev. X **13**, 011048 (2023).
[5] R. Abbott et al. (LIGO Scientific Collaboration, Virgo Collaboration, and KAGRA Collaboration), arXiv:2112.06861.
[6] H. Nakano, T. Narikawa, K. Oohara, K. Sakai, H. Shinkai, H. Takahashi, T. Tanaka, N. Uchikata, S. Yamamoto, T.S. Yamamoto, Phys. Rev. D. **99**, 124032 (2019).
[7] M. Saleem, S. Datta, K. G. Arun, and B. S. Sathyaprakash, Phys. Rev. D **105**, 084062 (2022).
[8] S. Datta, M. Saleem, K. G. Arun, and B. S. Sathyaprakash, arXiv:2208.07757.
[9] R. Niu, Z-C. Ma, J-M. Chen, C. Feng, W. Zhao, Results in Phys. **57**, 107407 (2024).
[10] D. Watarai, A. Nishizawa, K. Cannon, Phys. Rev. D **109** 084058 (2024).
[11] A. Hyvärinen, and E. Oja, Neural Networks **13** 411 (2000).
[12] A. Hyvärinen, J. Karhunen, and E. Oja, *Independent Component Analysis*, (John Wiley & Sons, 2001).
[13] A. J. Bell, T. J. Sejnowski, Neural Comput. **7**, 1129 (1995).
[14] R. De Rosa, L. A. Forte, F. Garufi, and L. Milano, Phys.

Rev. D **85**, 042001 (2012).
[15] T. Akutsu et al. (KAGRA collaboration), Prog. Theor. Exp. Phys. **2020**, 053F01 (2020).
[16] S. Morisaki, J. Yokoyama, K. Eda, and Y. Itoh, Proc. Japan Acad. B 92, 336 (2016) [arXiv:1605.01983 [gr-qc]]
[17] R. Abbott et al (LIGO Scientific Collaboration, Virgo Collaboration, and KAGRA Collaboration), Astrophys. J. Suppl. **267**, 29 (2023).